Available online at www.keaipublishing.com/en/journals/journal-of-magnesium-and-alloys/

ScienceDirect

Journal of Magnesium and Alloys xxx (xxxx) xxx

www.elsevier.com/locate/jma

Full Length Article

High strength and malleable lamellar-structured Mg/Mg_2Sn alloy

Xu-Jian Lin[1], Si-Mian Liu[1], Wei-Zhong Han*

Center for Advancing Materials Performance from the Nanoscale, State Key Laboratory for Mechanical Behavior of Materials, Xi'an Jiaotong University, Xi'an 710049, China

Received 11 March 2024; received in revised form 3 July 2024; accepted 16 July 2024
Available online xxx

Abstract

Lightweight Mg alloys are appealing as structural materials for improving energy efficiency in various applications. However, the tradeoff between strength and deformability of Mg at room temperature is a major obstacle to widespread use of Mg alloys. The plasticity of Mg is particularly related to $\langle c + a \rangle$ dislocations, which dominates c-axis strain, while it is rarely activated under ambient conditions because of a high critical resolved shear stress. Here, we prepare a lamellar-structured Mg/Mg_2Sn alloy consisting of two phases, Mg and Mg_2Sn, arranged alternately with high-density phase interfaces, which shows a synergy of high strength and deformability. High-density Mg/Mg_2Sn interfaces act as strong barriers for dislocations motion, obstructions for crack propagation, and efficient $\langle c + a \rangle$ dislocation sources, which contribute to the strengthening and plasticity of the laminated Mg/Mg_2Sn alloy. This unique interface-mediated plasticity provides a new pathway to improve the mechanical properties of hexagonal close-packed Mg alloys.

Keywords: Mg-Sn alloy; Lamellar structure; Interface; Malleable; $<c + a>$ dislocation.

1. Introduction

Mg alloys are considered as promising lightweight structural materials because of their low density [1]. However, their industrial applications are limited due to their low strength, low ductility, and tendency to corrode [2–9]. As a hexagonal close-packed (HCP) metal, the plastic deformation of Mg is primarily provided by dislocation slip and twinning [10,11]. Mg exhibits a dominant slip mode of $\{0001\}\ <1\bar{2}10>$ slip, commonly referred to as basal $\langle a \rangle$ slip, due to its low critical resolved shear stress (CRSS) of approximately 0.5 MPa at room temperature [12]. However, the basal $\langle a \rangle$ slip can only accommodate plasticity along the $<a>$-axis and it consists of only two independent slip systems. Therefore, Mg crystal cannot deform by basal $\langle a \rangle$ slip alone according to the Taylor-von Mises criterion for uniform plastic deformation, which requires at least five independent slip systems [13].

In HCP crystals, twinning acts as $a < c>$-axis deformation mechanism in addition to slip. However, unlike slip, all twin modes are unidirectional, and any given mode can either accommodate $<c>$-contraction or extension but not both [14,15]. Compared to twinning, the activation of $\langle c + a \rangle$ dislocation is the most favorable $<c>$-axis deformation mechanism [16–18]. The CRSS for pyramidal $\langle c + a \rangle$ dislocations in Mg alloys ranges from 30 to 80 MPa [19–23], which are significantly higher than that of the CRSS of basal $\langle a \rangle$ dislocation (0.5 MPa) [24]. As a result, $\langle c + a \rangle$ dislocations are difficult to initiate in Mg at ambient conditions. Even if they are activated, the $\langle c + a \rangle$ dislocation is still prone to decompose into sessile structures under thermally activated conditions and fails to contribute to plastic strain along the c-axis [25–27].

The activation energy barrier for the pyramidal-to-basal transition of the edge pyramidal II $\langle c + a \rangle$ dislocation is only about 0.5 eV for pure Mg [25]. Cross-slip of $\langle c + a \rangle$ screw dislocations could form dislocation loops and generate plasticity only if the activation energy for cross-slip is much lower than the activation energy barrier for the pyramidal-to-basal transition. However, the total activation energy required for

* Corresponding author.
E-mail address: wzhanxjtu@mail.xjtu.edu.cn (W.-Z. Han).
[1] These authors contributed equally to this work.

https://doi.org/10.1016/j.jma.2024.07.013

cross-slip is far beyond 0.5 eV, rendering cross-slip ineffective for preventing the negative consequences of the pyramidal-to-basal transition [25]. Promoting $\langle c + a \rangle$ dislocation cross-slip is an alternative method to improve the ductility of Mg alloys [28]. The addition of Ca, Mn, and Y as alloying elements can increase the cross-slip ability of $\langle c + a \rangle$ dislocations, leading to a substantial increase in plasticity in Mg alloys [29]. Furthermore, increasing the capacity for dislocation nucleation is another method to trigger the $\langle c + a \rangle$ dislocation. The addition of rare earth elements such as Y can effectively reduce the CRSS of pyramidal $\langle c + a \rangle$ dislocation, providing more nucleation sites of $\langle c + a \rangle$ dislocations [29].

Notably, the $\langle c + a \rangle$ screw dislocations move much faster than the $\langle c + a \rangle$ edge dislocations. The uncoordinated movement of screw vs. edge dislocation usually causes a poor dislocation self-multiplication efficiency [30,31]. To overcome the inefficient self-multiplication of $\langle c + a \rangle$ dislocations, one solution is to introduce more $\langle c + a \rangle$ dislocation sources. Phase interfaces have proved to be effective sources for $\langle c + a \rangle$ dislocations in zirconium [32–34]. In addition, atomistic simulations show that interface can mediate non-basal dislocation nucleation and hcp-to-bcc phase transformation under external loading when the basal slip systems are effectively suppressed [35]. The non-basal dislocation nucleation is closely related to the dynamic evolution of misfit dislocation patterns at the semi-coherent interface [32,35]. Interfaces can also increase dislocation storage and impede dislocation movement, thereby enhancing strength and deformability of materials [32,36]. To exploit the concept of interface engineering, directional solidification has been developed to fabricate interface-dominant Mg-based composites such as Mg/Mg_2Yb and Mg/Mg_2Ca eutectic alloys [37]. However, these high-strength layered Mg alloys exhibit near-zero plasticity at room temperature. Even when compressed at 400 °C, the layered composites remain quite brittle. Therefore, effectively initiating $\langle c + a \rangle$ dislocations to improve the deformability of Mg alloy via interface engineering still remains a challenge.

In this study, we prepare a two-phase Mg/Mg_2Sn composite with a high density of lamellar structures. The compressive behaviors of Mg-Sn alloys with different Sn contents and layer thicknesses are investigated. The Mg-Sn alloy with 36 wt.% Sn exhibits high compressive strength and good deformability. The underlying deformation mechanisms of Mg/Mg_2Sn alloys are analyzed in detail. In contrast to pure Mg and other nanolayered Mg alloys, the lamellar-structured Mg/Mg_2Sn alloys display higher strength and malleability via modulation of the nucleation of interfacial $\langle c + a \rangle$ dislocations, making lamellar Mg-Sn alloy as a promising lightweight structural material.

2. Experimental methods

2.1. Preparation of lamellar-structured Mg/Mg_2Sn alloy

Pure Mg (99.99 %) and pure Sn (99.99 %) are combined with varying mass ratios and placed into a 304 stainless steel canister with a height of 70 mm, radius of 8 mm, and wall thickness of 1.5 mm. The mixture is heated in a tube furnace under an Ar protective atmosphere at 800 °C for one hour. After melting and well-mixed of Sn and Mg, furnace cooling is used to make the Mg-9Sn, Mg-18Sn and Mg-36Sn alloys. According to the phase diagram of the Mg-Sn alloy, the eutectic component Mg-36Sn is likely expected to form a lamellar structure under equilibrium solidification conditions. In order to regulate the thickness of the lamellae of Mg/Mg_2Sn alloys, the Mg-36Sn alloys are cooled from 800 °C at three different rates, i.e., water-cooling, air-cooling, and furnace-cooling. Lamellar-structured Mg/Mg_2Sn alloy is formed only under specific compositional (Mg-36Sn) conditions, and adjusting the Sn content can effectively control the prevention of lamellar-structure formation. The lamellar-structured Mg/Mg_2Sn alloy has a density of approximately 2.4 g/cm^3, which is lighter than that of Al alloy.

2.2. Mechanical test

To compare with the Mg-Sn alloys, pure Mg is also selected for compressive test. Pure Mg, Mg-9Sn, Mg-18Sn and Mg-36Sn alloy for compressive test are fabricated into square columns with dimensions of 3 mm (length) × 3 mm (width) × 10 mm (height) by electrical discharge machining. The surface of the columns is carefully ground and polished by mechanical polishing. Compressive tests are performed on an MTS tensile machine at room temperature with a strain rate of $5 \times 10^{-4}\ s^{-1}$. Each Mg/Mg_2Sn alloy is tested for more than 3 times. The Micro-Vickers hardness is assessed using a 50 gf load, held for 15 s, and at least 15 spots are tested on both the normal and side surfaces.

2.3. Microstructure characterization

The initial and deformed microstructures of Mg/Mg_2Sn alloy are characterized using X-ray diffraction (XRD), scanning electron microscope (SEM), and transmission electron microscope (TEM). XRD is employed to identify the phase structure of Mg and Mg_2Sn. The XRD instrument utilized was the D8 ADVANCE model manufactured by Bruker in Germany. In this work, a copper target was chosen as the focal point, with a scanning range spanning from 10° to 90°, a scanning increment of 0.02°, and a scanning frequency of every 2 s. SEM is used to study the lamellar structures and fractured surface of the alloys. The SEM utilized in this work is the Hitachi SU6600. The operating voltage is 15 KV. All sample surfaces are mechanically polished before tests. TEM analysis is carried out to examine interface and dislocation structures in compressed samples. TEM samples are cut from deformed square columns and mechanically ground to a thickness of about 60 μm. Thin foils are further dimpled by ion-milling on a Gatan Precision Ion Polishing System, which is operated at 3 kV and with a final polishing beam angle of 4°

Please cite this article as: X.-J. Lin, S.-M. Liu and W.-Z. Han, High strength and malleable lamellar-structured Mg/Mg_2Sn alloy, Journal of Magnesium and Alloys, https://doi.org/10.1016/j.jma.2024.07.013

3. Results

Fig. 1 demonstrates the initial microstructures of Mg-9Sn, Mg-18Sn and Mg-36Sn alloys. The black matrix is Mg phase and the white precipitated phase is Mg_2Sn. As indicated by the arrows in Fig. 1(a), only a small quantity of Mg_2Sn phase precipitates locally in Mg when the Sn content is 9 wt.%. The Mg-9Sn alloy has an average micro-Vickers hardness of 54.8 ± 6.11 HV. With an increase in Sn content to 18 wt.%, more Mg_2Sn phase precipitates, forming an uneven Mg_2Sn/Mg composition (Fig. 1(b)). The average micro-Vickers hardness of the Mg-18Sn alloy increases to 60.3 ± 6.25HV. While in Mg-36Sn (Fig. 1(c)), the alloy undergoes a eutectic reaction resulting in the alternate arrangement of Mg_2Sn and Mg phases, forming a uniformly lamellar structure. The average micro-Vickers hardness is 83.6 ± 3.15 HV. Fig. 1(d) shows the compressive stress-strain curves of pure Mg and Mg-Sn alloys with varying Sn contents. Pure Mg exhibits an ultimate compressive strength of 165 MPa and the highest fracture strain of 24.1 %. Mg-9Sn alloy exhibits a similar fracture strain but a higher ultimate strength of 182 MPa. The ultimate strength of Mg-18Sn increases to 196 MPa while the compressive strain decreases from 23.6 % to 17.5 % compared with Mg-9Sn. The compressive strength of Mg-36Sn alloy significantly increases to 322 MPa with a decrease of compressive fracture strain to 15.4 %. Fig. 1(e) plots the yield strength, ultimate compressive strength and fracture strain of pure Mg and Mg-Sn alloys. As the content of Sn increases from 0 to 36 %, the yield strength sharply increases from 16.9 MPa to 157.6 MPa, and the ultimate compressive strength rises from 152.3 MPa to 293 MPa. However, the fracture strain falls from 25.8 % to 15.4 %. The mechanical properties of Mg-Sn alloys vary significantly due to large differences in layer thickness. Compared with the lamellar Mg/Mg_2Yb alloy and Mg/Mg_2Ca alloys [37], the layered Mg-36Sn alloys show a significant improvement in deformability, as shown in Fig. 1(d).

Fig. 2 reveals the fracture surface of pure Mg and Mg-Sn alloys. The fracture surface of pure Mg shows obvious slip traces from two different directions, as indicated by the enlarged SEM images in Fig. 2(b) and (c). Similarly, many slip traces are observed in the Mg phase of Mg-9Sn alloy (Fig. 2(d)). A crack is observed at the interface between Mg and Mg_2Sn (Fig. 2(e)). Fig. 2(f) shows several slip bands passing through the Mg/Mg_2Sn layered structure, forming elongated micro-cracks in Mg_2Sn phases. The deformation behavior of Mg-18Sn is comparable to that of Mg-9Sn. A large crack separates the Mg matrix from the Mg/Mg_2Sn region (Fig. 2(h)). Sharp microcracks are also found to traverse the Mg_2Sn phase, as shown in Fig. 2(i). In the case of layered

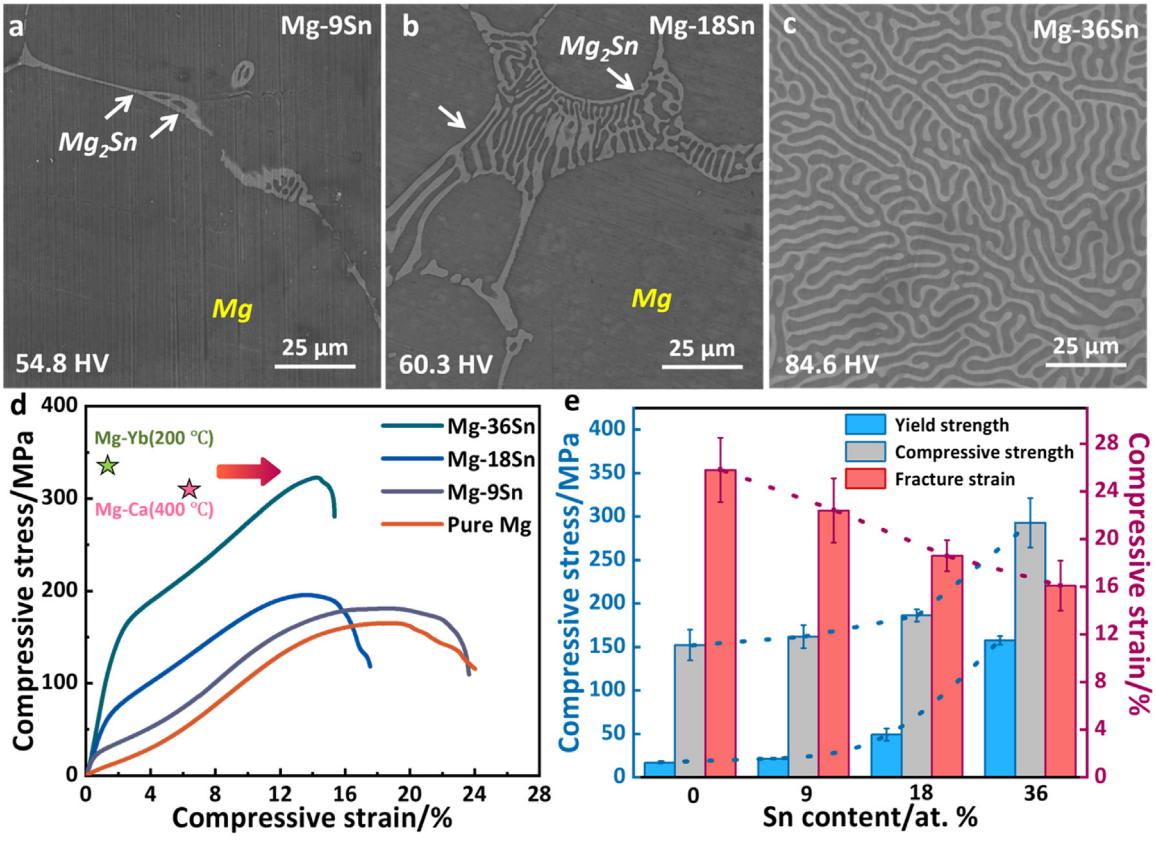

Fig. 1. Mechanical properties and microstructures of Mg-Sn alloys with different Sn contents. Initial microstructures of (a) Mg-9Sn, (b) Mg-18Sn, (c) Mg-36Sn. (d) Compressive stress-strain curves for pure Mg and Mg-Sn alloys. The green star shows the strength and compression strain of lamellar Mg/Mg_2Yb alloy at 200 °C [37]. The red star marks the strength and compression strain of lamellar Mg/Mg_2Ca alloy at 400 °C [37]. (e) Variation of strength and compressive strain with Sn contents.

Please cite this article as: X.-J. Lin, S.-M. Liu and W.-Z. Han, High strength and malleable lamellar-structured Mg/Mg_2Sn alloy, Journal of Magnesium and Alloys, https://doi.org/10.1016/j.jma.2024.07.013

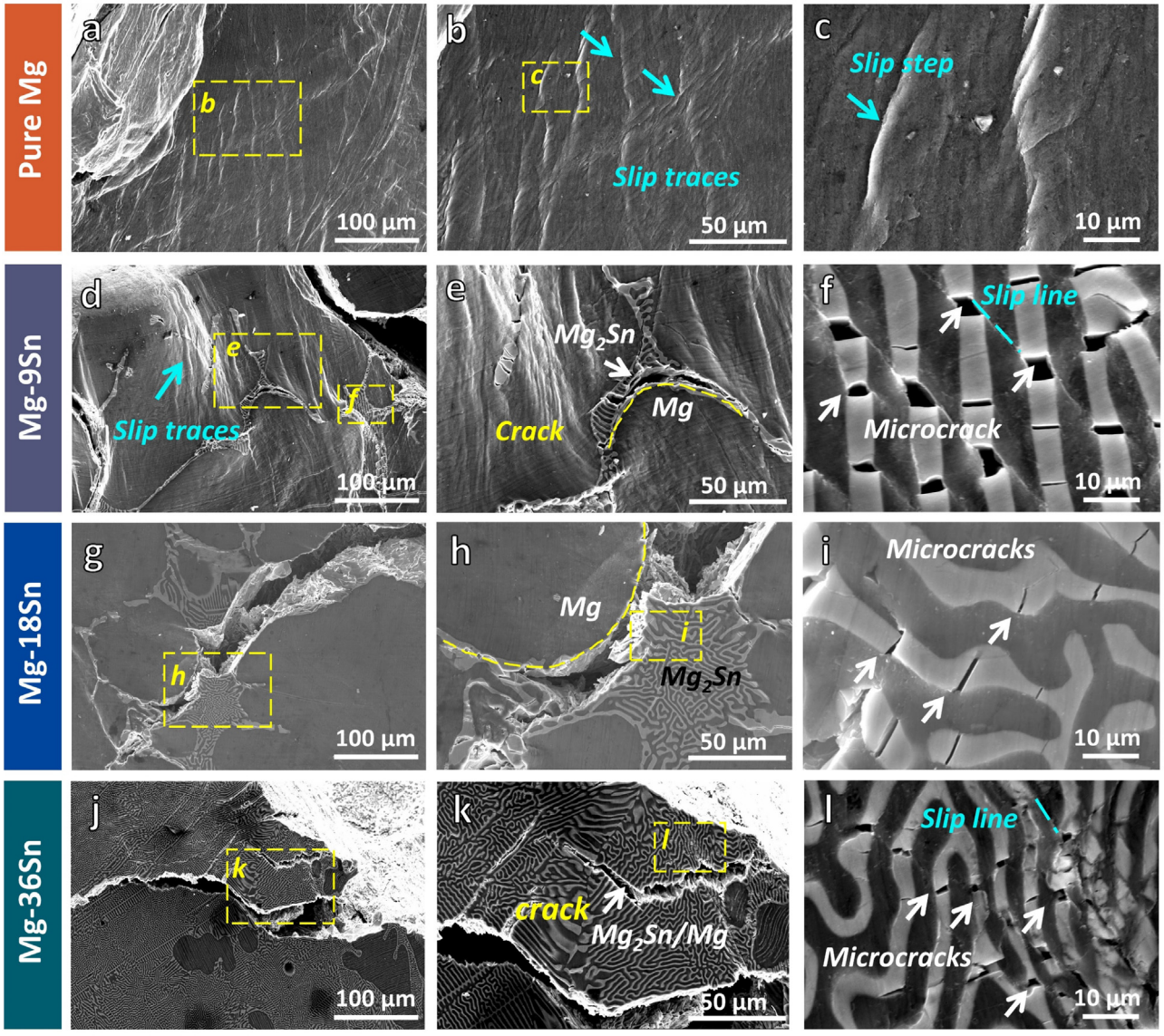

Fig. 2. Typical SEM images of surface deformation morphologies of pure Mg (a-c), Mg-9Sn (d-f), Mg-18Sn (g-i), Mg-36Sn (j-l).

Mg-36Sn, the crack spreads across phase interface rather than along it (Fig. 2(k)). The crack extension pass is more curved and crosses the Mg/Mg_2Sn interface. The localized deformation mode is a typical deformation mechanism in heterogeneous metal-structured materials, in which the malleable Mg phase restricts the growth of microcracks in the brittle Mg_2Sn phase.

In order to investigate the effect of layer spacing on the mechanical properties of Mg-36Sn alloys, the lamellar Mg/Mg_2Sn alloys with different layer spacing were prepared using three different cooling rates: water-cooling, air-cooling and furnace-cooling. After water-cooling (Fig. 3(a)), the average layer spacing of the Mg phase is 0.26±0.03 μm with ultra-fine Mg_2Sn phases. The layer thickness of the Mg phase after air-cooling and furnace-cooling is about 0.45±0.04 μm and 2.5 ± 0.08 μm, respectively (Fig. 3(b-c)). The average micro-Vickers hardness is 124.5 ± 10.53 HV for the water-cooled sample, 84.3 ± 2.49 HV for the air-cooled sample and 83.6 ± 3.15 HV for the furnace-cooled sample. Fig. 3(d) shows the compressive stress-strain curves for the lamellar Mg-36Sn alloys. Water-cooled Mg-36Sn alloy shows the highest strength but the lowest fracture stain. Furnace-cooled Mg-36Sn alloy has improved plasticity and a noticeable work-hardening stage. The compressive strength and fracture strain versus layer thickness of the Mg phase are shown in Fig. 3(e). As the spacing of the lamellar structure becomes thicker, the plasticity of Mg-36Sn significantly increases with a slight decrease in strength. Briefly, the lamellar Mg/Mg_2Sn with layer spacing of 2.5 μm displays the best combination of strength and malleability within the three samples. The phase structures were characterized using XRD, as shown in Fig. 3(f). An increasing cooling rate results in a greater number of Mg_2Sn phase with various orientations. Because of the very fine layer structures in water-cooled and air-cooled samples, only XRD peaks of Mg_2Sn phase appear, while the XRD peaks for Mg phase are very weak, as shown in Fig. 3(f).

Please cite this article as: X.-J. Lin, S.-M. Liu and W.-Z. Han, High strength and malleable lamellar-structured Mg/Mg_2Sn alloy, Journal of Magnesium and Alloys, https://doi.org/10.1016/j.jma.2024.07.013

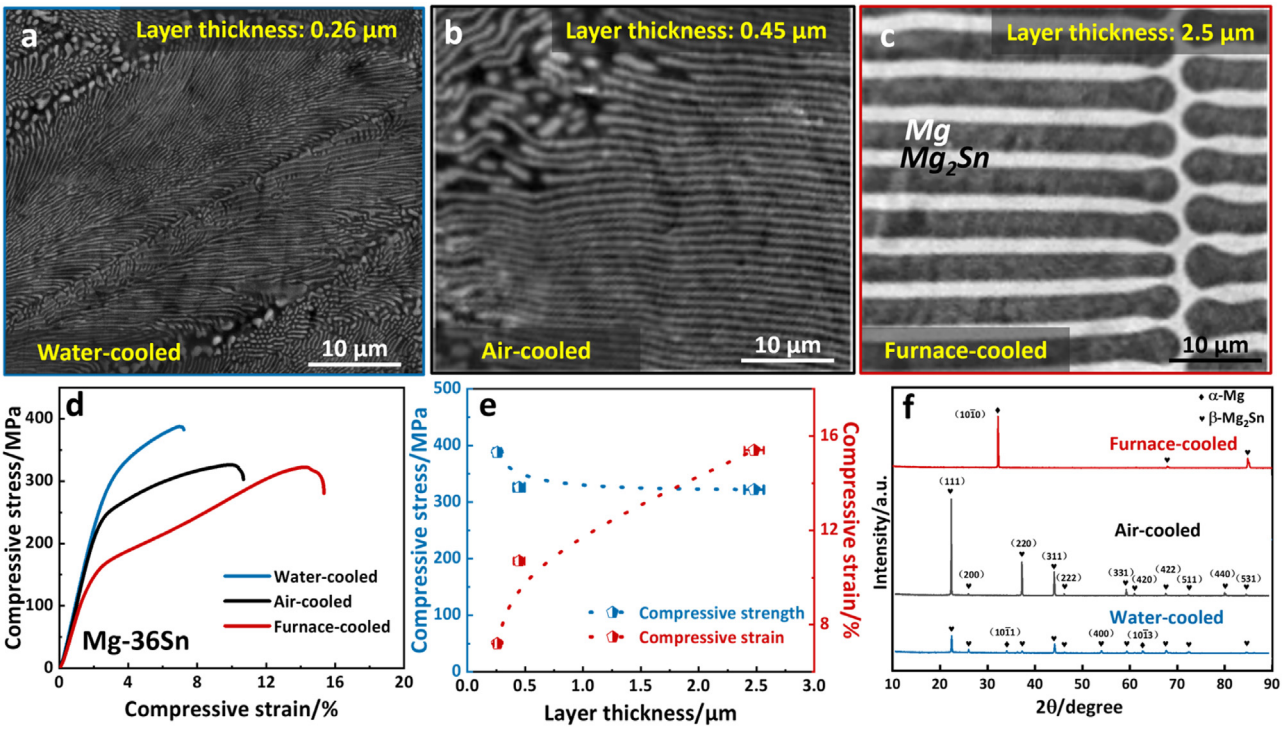

Fig. 3. Mechanical properties and microstructures of Mg-36Sn alloy with different layer thickness. Microstructures of Mg-36Sn with a layer thickness of (a) 0.26 μm, (b) 0.45 μm, (c) 2.5 μm, (d) Compressive stress-strain curves of Mg-36Sn alloys with different cooling rates. (e) Compressive strength and fracture strain versus layer thickness of Mg phase. (f) XRD results of Mg-36Sn alloys with different cooling rates. Because of the ultrafine layer structures, the XRD peak for Mg is weak for water-cooled and air-cooled samples.

Fig. 4 shows the fracture surface of Mg-36Sn alloys with different cooling rates. No slip traces or microcracks are observed in the water-cooled Mg-36Sn alloy (Fig. 4(b)). The crack is sharp and propagates across the Mg/Mg_2Sn phase interface (Fig. 4(c)). The fracture of the air-cooled Mg-36Sn alloy is similar to that of the water-cooled Mg-36Sn alloy, with no slip traces are detected, while some microcracks are observed in the Mg_2Sn phase, as shown in Fig. 4(f). In contrast, numerous slip traces are detected in the furnace-cooled Mg-36Sn alloy (Fig. 4(h)), indicating better deformability, as shown in Fig. 3(a). Moreover, the broader morphology of the microcracks suggests a greater ability to impede cracking expansion as the lamella thickness increases.

To understand the plastic deformation mechanism of lamellar-structured Mg/Mg_2Sn alloy, the furnace-cooled Mg-36Sn is compressed to different strains and characterized using SEM and TEM. Fig. 5 shows the surface morphology of Mg-36Sn after compressive strains of 2.8 %, 5.5 %, and 9.5 %. At 2.8 % strain, the soft Mg phase deforms first and forms slip traces (Fig. 5(b)), which across the Mg/Mg_2Sn interface (Fig. 5(c)). At 5.5 % strain, the Mg_2Sn phase starts to sprout microcracks (Fig. 5(f)). At 9.5 % strain, numerous tiny microcracks interlink to form large cracks across the layers, as shown in Fig. 5(h) and (i).

The dislocation structures accumulated at different stages in the compressed Mg-36Sn alloy are shown in Fig. 6. Dislocation analysis was performed using the two-beam condition with $\vec{g}$=0002 diffraction vector. Under this imaging condition, ⟨a⟩ dislocations are out of contrast while ⟨$c + a$⟩ dislocations are visible. The yellow dotted line refers to the Mg/Mg_2Sn phase interface. At compressive strain of 2.8 %, several short ⟨$c + a$⟩ dislocations are observed in the Mg phase near the interface. The density of ⟨$c + a$⟩ dislocation increases after a compressive strain of 5.5 %. At 9.5 % strain, the ⟨$c + a$⟩ dislocation becomes longer (Fig. 6(c)). A small-angle grain boundary (SAGB) forms because of the accumulation of ⟨a⟩ dislocations near the interphase, as shown by the bright-field and dark-field TEM images in Fig. 6(d). After a compressive strain of 15.2 %, the sample fractures completely. The density of ⟨$c + a$⟩ dislocations near the interface is very high (Fig. 6(e)). More straight and long dislocations with zig-zag segments are remained (Fig. 6(f)). The straight segments are parallel to the (0001) basal plane trace, and the zig-zag dislocation segments are parallel to different pyramidal planes. A SAGB is also observed near the interphase in Mg layer, as shown in Fig. 6(f).

Fig. 7 further characterizes the ⟨$c + a$⟩ dislocations near the Mg/Mg_2Sn interface in Mg-36Sn alloy when the strain reaches 9.5 % and 15.2 %. At compressive strain of 9.5 %, many curved ⟨$c + a$⟩ dislocation lines are observed near the interface, as indicated by the yellow lines in Fig. 7(a). They are mixed dislocations and accumulate at the phase interface. Many dislocations pile up at the interface (Fig. 7(b)). After the fracture of Mg/Mg_2Sn alloy, the dislocations near the interphase become long and straight. These dislocations are the edge parts of the ⟨$c + a$⟩ dislocation (Fig. 7(c)). Curved

Please cite this article as: X.-J. Lin, S.-M. Liu and W.-Z. Han, High strength and malleable lamellar-structured Mg/Mg_2Sn alloy, Journal of Magnesium and Alloys, https://doi.org/10.1016/j.jma.2024.07.013

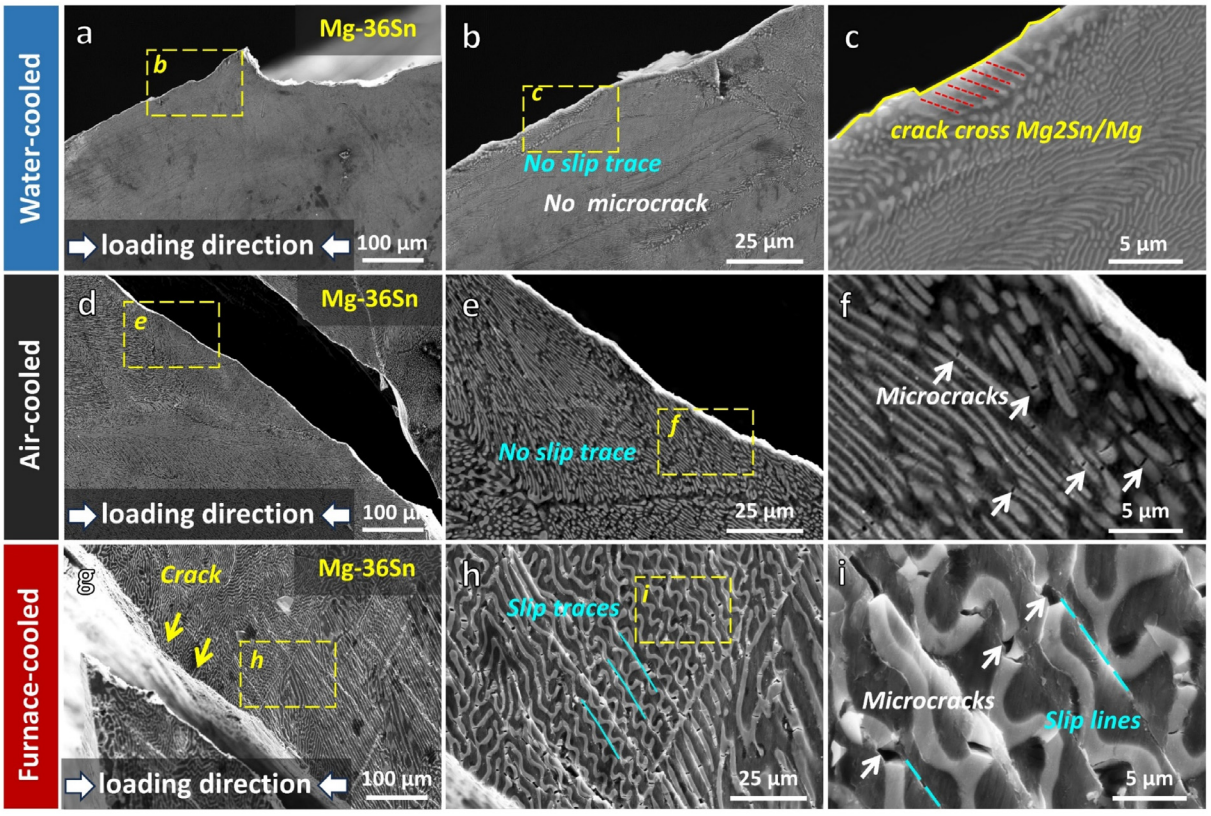

Fig. 4. Fracture surface of Mg-36Sn alloys with different cooling conditions. (a-c) Water-cooled sample, (d-f) Air-cooled sample, and (g-i) Furnace-cooled sample.

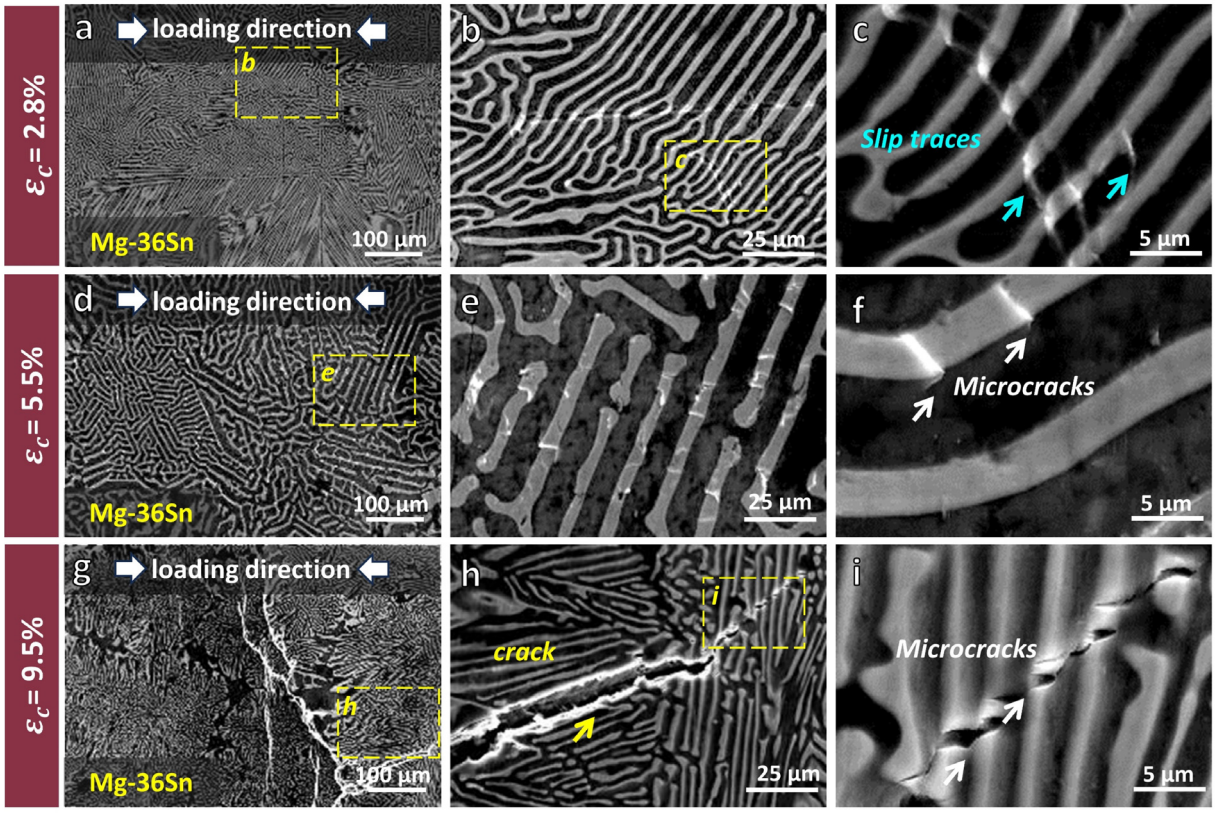

Fig. 5. Surface deformation features of furnace-cooled Mg-36Sn alloy with different compressive strains. (a-c) ε_c= 2.8 %. (d-f) ε_c=5.8 %. (g-i) ε_c= 9.5 %.

Please cite this article as: X.-J. Lin, S.-M. Liu and W.-Z. Han, High strength and malleable lamellar-structured Mg/Mg_2Sn alloy, Journal of Magnesium and Alloys, https://doi.org/10.1016/j.jma.2024.07.013

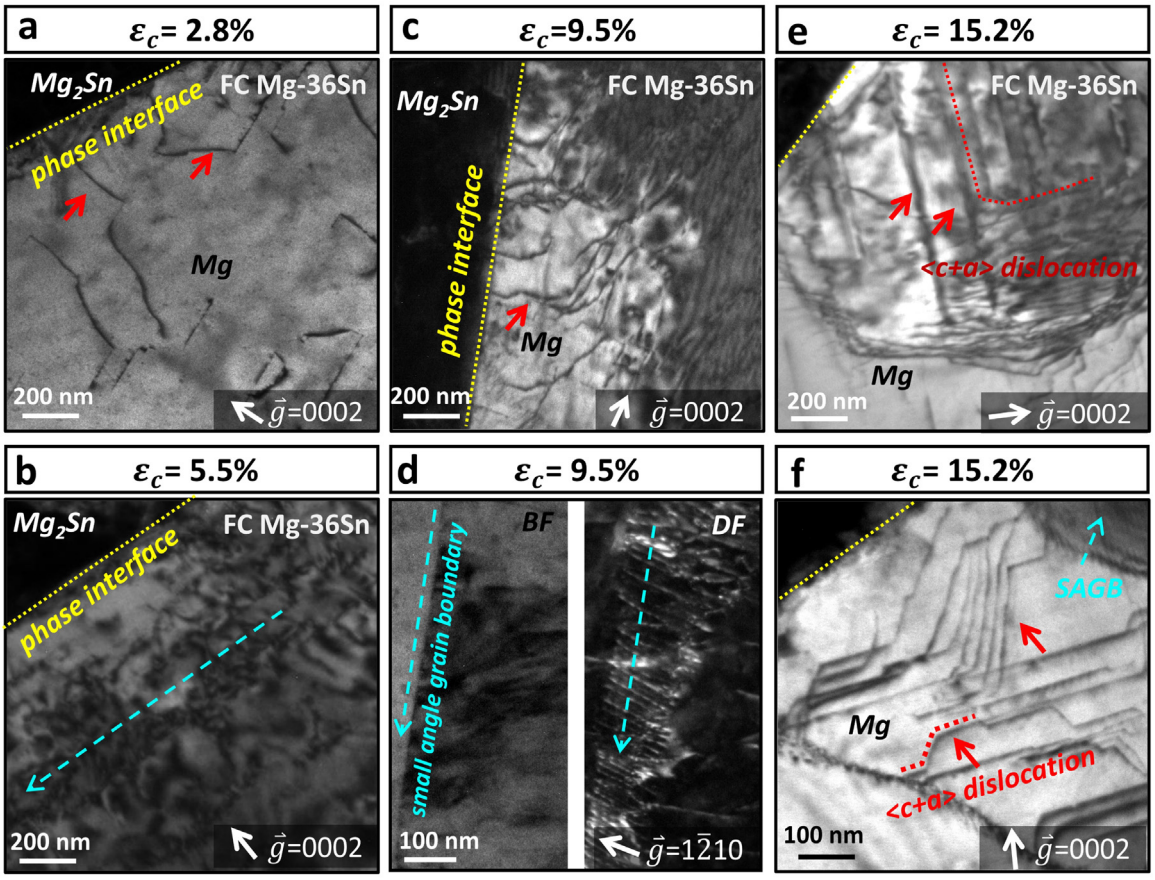

Fig. 6. Dislocation structures in compressed furnace cooled Mg-36Sn. (a) ε_c=2.8 %. (b) ε_c=5.5 %. (c-d) ε_c=9.5 %. (e-f) ε_c=15.2 %.

dislocations in blue color are connected at the front end of the edge dislocation, as indicated in Fig. 7(c). The curved dislocations have mixed features, with more screw components. During deformation, easy glide screw $\langle c+a \rangle$ dislocations lead less mobile long straight edge $\langle c+a \rangle$ dislocations forward [38]. The edge part of the $\langle c+a \rangle$ dislocation drags the glide of whole dislocation line and hinders the dislocation from evolving into an efficient dislocation source [30]. The Mg/Mg_2Sn interfaces act as a source of dislocations that emit the $\langle c+a \rangle$ dislocations, as shown in Fig. 7(c) and (d). Although the $\langle c+a \rangle$ dislocations have a low dislocation source efficiency, but the numerous interfaces could effectively provide high density of $\langle c+a \rangle$ dislocations to mediate plasticity.

4. Discussion

4.1. Effect of interface on $\langle c+a \rangle$ dislocation nucleation

Basal $\langle a \rangle$ dislocations are prevalent in pure Mg while the ductility of Mg is particularly dependent on $\langle c+a \rangle$ dislocations, which control the c-axis strain [25]. $\langle c+a \rangle$ dislocations are critical defects that provide plasticity and are generally triggered under high strain rates or high temperatures loading [38]. To overcome the weakness of poor deformability due to the lack of $\langle c+a \rangle$ dislocation, numerous Mg/Mg_2Sn interfaces are introduced into Mg alloy to improve the deformability. A high density of $\langle c+a \rangle$ dislocations is captured in proximity to the Mg/Mg_2Sn interface, which is higher than that observed in the intermediate region, as seen in Fig. 7(b). This suggests that the interface has a superior ability to nucleate and emit $\langle c+a \rangle$ dislocations compared to the grain interior. Mixed dislocations are observed close to the interface at the earlier stage of loading (see Fig. 6(a)), indicating that the $\langle c+a \rangle$ dislocations are nucleating from the interfaces. With increasing of strain (see Fig. 7(d)), edge $\langle c+a \rangle$ dislocations are still remained near the phase interface. This is because the mobility of $\langle c+a \rangle$ screw dislocations is higher than that of $\langle c+a \rangle$ edge dislocations [30], and the screw $\langle c+a \rangle$ dislocations glide forward while the edge $\langle c+a \rangle$ dislocations are left (see Fig. 7(c)). The different kinematic properties of the screw $\langle c+a \rangle$ dislocations and the edge $\langle c+a \rangle$ dislocations lead to a poor dislocation self-multiplication efficiency [30]. However, the multiple Mg/Mg_2Sn interfaces serve as efficient sources of $\langle c+a \rangle$ dislocations and eliminate the $\langle c+a \rangle$ dislocation starvation. It is worth point out that the Mg/Mg_2Sn interfaces can produce a large number of $\langle c+a \rangle$ dislocations to coordinate plastic deformation via increasing the number of $\langle c+a \rangle$ dislocation sources rather than improving the mobility of $\langle c+a \rangle$ dislocations.

Please cite this article as: X.-J. Lin, S.-M. Liu and W.-Z. Han, High strength and malleable lamellar-structured Mg/Mg_2Sn alloy, Journal of Magnesium and Alloys, https://doi.org/10.1016/j.jma.2024.07.013

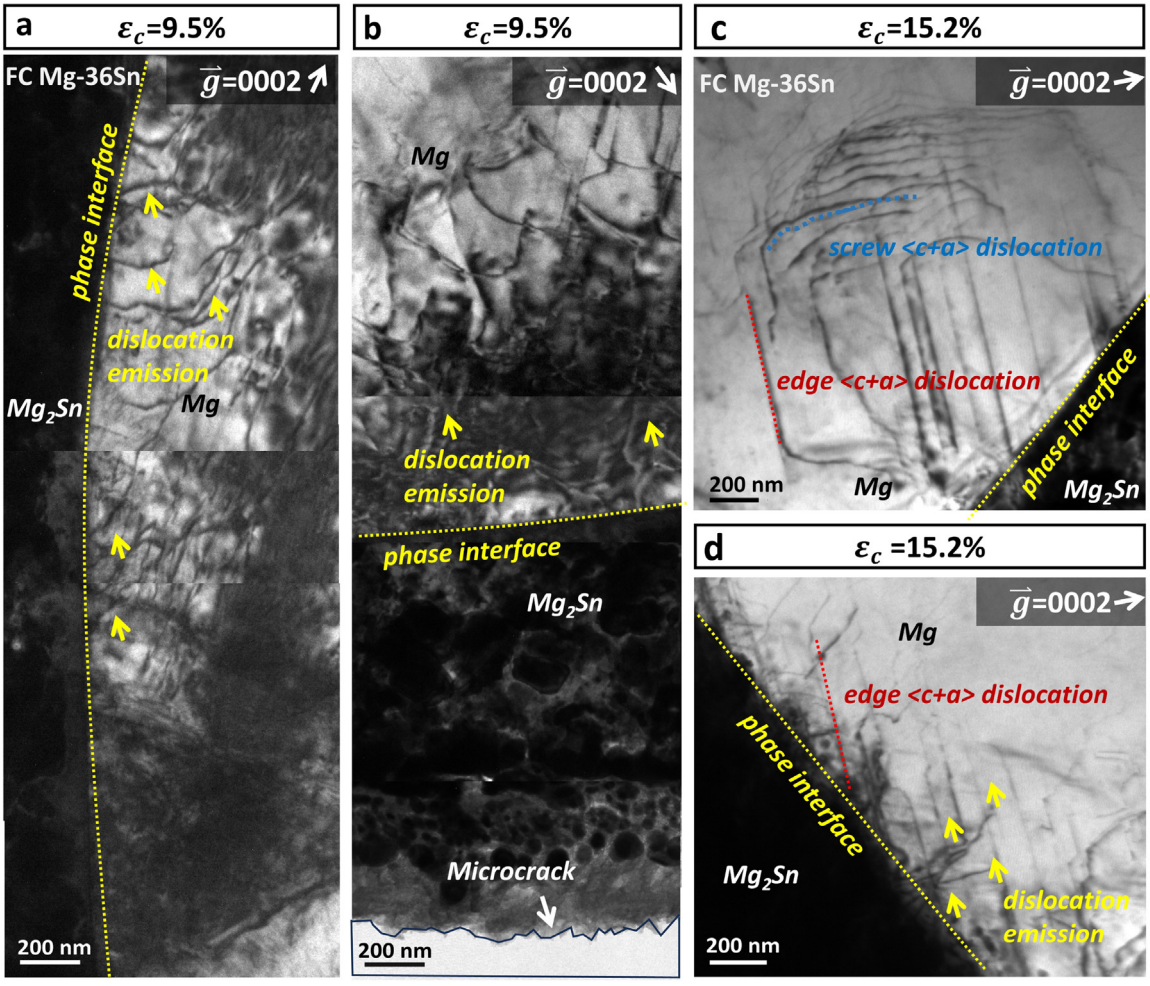

Fig. 7. Emission of $\langle c + a \rangle$ dislocations from Mg/Mg_2Sn interface during compression of furnace cooled Mg-36Sn alloy. (a-b) $\langle c + a \rangle$ dislocations accumulated at Mg/Mg_2Sn interface at ε_c=9.5 %. (c-d) $\langle c + a \rangle$ dislocations emitted from Mg/Mg_2Sn interface at ε_c=15.2 %.

4.2. Effect of interface on strength and deformability

The compressive strength of lamellar-structured Mg-36Sn is significantly higher than that of Mg-9Sn and Mg-18Sn alloys due to an increase in the volume fraction of high-strength Mg_2Sn phases. Furthermore, the Mg/Mg_2Sn phase interface could impedes dislocation movement and promote dislocation pile-up and storage, further enhancing the strength of lamellar-structured Mg-36Sn. In addition, the interfaces could also effectively prevent crack in brittle Mg_2Sn phases further propagation, delaying the eventual failure of the sample. In Mg-9Sn and Mg-18Sn alloys, the cracks propagate along the grain boundary due to stress concentration at the interface [32] and a relatively lower density of laminar structures. While in lamellar-structured Mg-36Sn alloy, greater stress is required for the expansion of cracks to cross multiple Mg/Mg_2Sn interfaces. The strong obstruction on cracking imposed by numerous Mg/Mg_2Sn interfaces also contribute to the high compressive strength of Mg-36Sn alloy. The presence of cracks only in the Mg_2Sn layer indicates that the Mg layer effectively blunts the extension of the microcracks. Interface-mediated $\langle c + a \rangle$ dislocations make micro-scale Mg layers with excellent deformability. The deformable Mg phase coordinates the plastic deformation to a greater extent, preventing the expansion of these microcracks. The abundant Mg/Mg_2Sn interface obstructs crack extension (see Fig. 5(h)), which contribute to the deformability of whole sample as well. The high density of Mg/Mg_2Sn interfaces not only effectively obstructs the glide of dislocations, but also stimulates numerous of $\langle c + a \rangle$ dislocations and blunt the cracking, thus enhance the strength and malleability of the Mg-36Sn alloy simultaneously. The lamellar-structured Mg/Mg_2Sn alloy involves both hard and soft phases, allowing for a combination of good deformability and high strength.

5. Conclusions

In this study, we successfully synthesis a lamellar-structured Mg/Mg2Sn alloy with high compressive strength and good deformability. Lamellar-structured Mg/Mg_2Sn alloys contain Mg and Mg_2Sn phases arranged alternately. During compression, the brittle Mg_2Sn phase generates multiple microcracks, and the microscale malleable Mg phase coordinates the plastic deformation and prevents the expansion

Please cite this article as: X.-J. Lin, S.-M. Liu and W.-Z. Han, High strength and malleable lamellar-structured Mg/Mg_2Sn alloy, Journal of Magnesium and Alloys, https://doi.org/10.1016/j.jma.2024.07.013

of microcracks. Such a heterogeneous Mg/Mg_2Sn alloy has a good combination of deformability and high compressive strength. The Mg/Mg_2Sn interfaces not only obstruct the glide of dislocations and crack propagation, and contribute to the high strength, but also serve as effective sources of $\langle c + a \rangle$ dislocations, and improve the deformability. This new mechanism of interface-mediated deformation provides a unique approach to enhancing the mechanical properties of magnesium alloys and even other alloy systems.

Declaration of competing interest

The authors declare the following financial interests/personal relationships which may be considered as potential competing interests:

A patent has been filed for the method of preparing the lamellar-structured Mg/Mg_2Sn Alloy

CRediT authorship contribution statement

Xu-Jian Lin: Writing – original draft, Validation, Investigation, Formal analysis, Data curation. **Si-Mian Liu:** Methodology, Investigation, Formal analysis, Data curation. **Wei-Zhong Han:** Conceptualization, Formal analysis, Funding acquisition, Investigation, Methodology, Project administration, Resources, Supervision, Validation, Visualization, Writing – review & editing.

Acknowledgments

This research was supported by the National Natural Science Foundation of China (Grant Nos. 51471128 and 52301019).

References

[1] T.M. Pollock, Science 328 (2010) 986–987, doi:10.1126/science.1182848.
[2] S. Seetharaman, A. Almajid, M. Gupta, Metals 5 (2014) 1–39, doi:10.3390/met5010001.
[3] L.Y. Chen, J.Q. Xu, H. Choi, M. Pozuelo, X. Ma, S. Bhowmick, J.M. Yang, S. Mathaudhu, X.C. Li, Nature 528 (2015) 539–543, doi:10.1038/nature16445.
[4] S. Henes, V. Gerold, Z. Metall. 53 (1962) 743, doi:10.1515/ijmr-1962-531202.
[5] T.T. Sasaki, K. Oh-ishi, T. Ohkubo, K. Hono, Scr. Mater. 55 (2006) 251–254, doi:10.1016/j.scriptamat.2006.04.005.
[6] C. Liu, H. Chen, J.F. Nie, Scr. Mater. 123 (2016) 5–8, doi:10.1016/j.scriptamat.2016.05.035.
[7] M. Zhang, W.Z. Zhang, G.Z. Zhu, Scr. Mater. 59 (2008) 866–869, doi:10.1016/j.scriptamat.2008.06.033.
[8] T.T. Sasaki, F.R. Elsayed, T. Nakata, T. Ohkubo, S. Kamado, K. Hono, Acta Mater. 99 (2015) 176–186, doi:10.1016/j.actamat.2015.06.060.
[9] T.T. Sasaki, K. Yamamoto, T. Honma, S. Kamado, K. Hono, Scr. Mater. 59 (2008) 1111–1114, doi:10.1016/j.scriptamat.2008.07.042.
[10] T.T. Sasaki, J.D. Ju, K. Hono, K.S. Shin, Scr. Mater. 61 (2009) 80–83, doi:10.1016/j.scriptamat.2009.03.014.
[11] Z.Z. Shi, W.Z. Zhang, X.F. Gu, Philos. Mag. 92 (2012) 1071–1082, doi:10.1080/14786435.2011.640294.
[12] C.L. Mendis, C.J. Bettles, M.A. Gibson, S. Gorsse, C.R. Hutchinson, Mag. Lett. 86 (2006) 443–456, doi:10.1080/09500830600871186.
[13] X.F. Huang, W.Z. Zhang, Mater. Sci. Eng. A 552 (2012) 211–221, doi:10.1016/j.msea.2012.05.033.
[14] A.A. Nayeb-Hashemi, J.B. Clark, Pearson's Handbook of Crystallographic Data For Intermetallic Phases, ASM International Metals Park, OH, 1988.
[15] J. Koike, T. Kobayashi, T. Mukai, H. Watanabe, M. Suzuki, K. Maruyama, K. Higashi, Acta Mater. 51 (2003) 2055–2065, doi:10.1016/S1359-6454(03)00005-3.
[16] Y.K. Kamado, Sci. Eng. Compos. Mater. 6 (1997) 159–167, doi:10.1515/SECM.1997.6.3.159.
[17] M.H. Yoo, Metall. Mater. Trans. A 12 (1981) 409–418, doi:10.1007/BF02648537.
[18] S. Agnew, D. Brown, C. Tome, Acta Mater. 54 (2006) 4841–4852, doi:10.1016/j.actamat.2006.06.020.
[19] J. Zhang, S.P. Joshi, J. Mech. Phys. Solids 60 (2012) 945–972, doi:10.1016/j.jmps.2012.01.005.
[20] T. Obara, H. Yoshinga, S. Morozumi, Acta Metall. 21 (1973) 845–853, doi:10.1016/0001-6160(73)90141-7.
[21] B. Syed, J. Geng, R.K. Mishra, K.S. Kumar, Scr. Mater. 67 (2012) 700–703, doi:10.1016/j.scriptamat.2012.06.036.
[22] C.M. Byer, B. Li, B. Cao, K.T. Ramesh, Scr. Mater. 62 (2010) 536–539, doi:10.1016/j.scriptamat.2009.12.017.
[23] K.Y. Xie, Z. Alam, A. Caffee, K.J. Hemker, Scr. Mater. 112 (2016) 75–78, doi:10.1016/j.scriptamat.2015.09.016.
[24] A. Akhtar, E. Teghtsoonian, Acta Metall. 17 (1969) 1339–1349, doi:10.1016/0001-6160(69)90151-5.
[25] Z. Wu, W.A. Curtin, Nature 526 (2015) 62–67, doi:10.1038/nature15364.
[26] Z. Wu, W.A. Curtin, Scr. Mater. 116 (2016) 104–107, doi:10.1016/j.scriptamat.2016.01.041.
[27] R. Ahmad, Z. Wu, S. Groh, W.A. Curtin, Scr. Mater. 155 (2018) 114–118, doi:10.1016/j.scriptamat.2018.06.026.
[28] K. Srivastava, S.I. Rao, J.A. El-Awady, Acta Mater. 161 (2018) 182–193, doi:10.1016/j.actamat.2018.09.010.
[29] Z. Wu, R. Ahmad, B. Yin, S. Sandlöbes, W.A. Curtin, Science 359, (2018) 447–452, doi:10.1126/science.aap8716.
[30] Y. Lu, Y.H. Zhang, E. Ma, W.Z. Han, Proc. Natl. Acad. Sci. U.S.A 118 (2021) e21105961182021, doi:10.1073/pnas.2110596118.
[31] H.M. Liu, Y.G. Chen, Y.B. Tang, J. Alloys Compd. 440 (2007) 122126, doi:10.1016/j.jallcom.2006.09.024.
[32] J.W. Zhang, I.J. Beyerlein, W.Z. Han, Phys. Rev. Lett 122 (2019) 255501, doi:10.1103/PhysRevLett.122.255501.
[33] A. Misra, J.P. Hirth, P.G. Hoagland, Acta Mater. 53 (2015) 48174824, doi:10.1016/j.actamat.2005.06.025.
[34] C.X. Huang, Y.F. Wang, X.L. Ma, Mater. Today 21 (2018) 713719, doi:10.1016/j.mattod.2018.03.006.
[35] X.P. Shen, B.N. Yao, Z.R. Liu, D Legut, H.J. Zhang, R.F. Zhang, Int. J. Plast. 146 (2021) 103105, doi:10.1016/j.ijplas.2021.103105.
[36] L.L. Li, Y.Q. Su, I.J. Beyerlein, W.Z. Han, Sci. Adv. 6 (2020) 39, doi:10.1126/sciadv.abb6658.
[37] K. Hagihara, K. Miyoshi, J. Magnes. A. 10 (2021) 492–500, doi:10.1016/j.jma.2021.02.006.
[38] B.Y. Liu, F. Liu, N. Yang, X.-B. Zhai, L. Zhang, Y. Yang, B. Li, J. Li, E. Ma, J.F. Nie, Z.W. Shan, Science 365 (2019) 73–75, doi:10.1126/science.aaw2843.